THE JOURNAL OF PHYSICAL CHEMISTRY C

Article

Cite This: J. Phys. Chem. C 2017, 121, 24657-24668

pubs.acs.org/JPCC

Orientation-Dependent Work-Function Modification Using Substituted Pyrene-Based Acceptors

O. T. Hofmann,[*,†] H. Glowatzki,[‡] C. Bürker,[§] G. M. Rangger,[†] B. Bröker,[∥] J. Niederhausen,[‡] T. Hosokai,[⊥] I. Salzmann,[∥,▽] R.-P. Blum,[∥] R. Rieger,[#] A. Vollmer,[‡] P. Rajput,[¶] A. Gerlach,[§] K. Müllen,[#,△] F. Schreiber,[§] E. Zojer,[†] N. Koch,[‡,∥,○] and S. Duhm[*,○]

[†]Institute of Solid State Physics, NAWI Graz, Graz University of Technology, Petersgasse 16, 8010 Graz, Austria

[‡]Helmholtz-Zentrum Berlin für Materialien und Energie GmbH, Albert-Einstein-Str. 15, 12489 Berlin, Germany

[§]Institut für Angewandte Physik, Universität Tübingen, Auf der Morgenstelle 10, Tübingen 72076, Germany

[∥]Institut für Physik & IRIS Adlershof, Humboldt-Universität zu Berlin, Newtonstraße 15, 12389 Berlin, Germany

[⊥]National Institute of Advanced Industrial Science and Technology (AIST), Tsukuba Central 2, 1-1-1 Umezono, Tsukuba, Ibaraki 305-8568, Japan

[#]Max Planck Institut für Polymerforschung, Ackermannweg 10, 55128 Mainz, Germany

[¶]Atomic & Molecular Physics Division, Bhabha Atomic Research Centre, Trombay, Mumbai 400085, India

[△]Institute of Physical Chemistry, Johannes Gutenberg University Mainz, Duesbergweg 10-14, Mainz, Germany

[○]Jiangsu Key Laboratory for Carbon-Based Functional Materials & Devices and Institute of Functional Nano & Soft Materials (FUNSOM), Soochow University, 199 Ren-Ai Road, Suzhou 215123, P.R. China

[▽]The Institute of Solid State Physics, The University of Tokyo, Kashiwanoha 5-1-5, Kashiwa, Chiba 277-8581, Japan

Supporting Information

ABSTRACT: The adsorption of molecular acceptors is a viable method for tuning the work function of metal electrodes. This, in turn, enables adjusting charge injection barriers between the electrode and organic semiconductors. Here, we demonstrate the potential of pyrene-tetraone (PyT) and its derivatives dibromopyrene-tetraone (Br-PyT) and dinitropyrene-tetraone (NO_2-PyT) for modifying the electronic properties of Au(111) and Ag(111) surfaces. The systems are investigated by complementary theoretical and experimental approaches, including photoelectron spectroscopy, the X-ray standing wave technique, and density functional theory simulations. For some of the investigated interfaces the trends expected for Fermi-level pinning are observed, i.e., an increase of the metal work function along with increasing molecular electron affinity and the same work function for Au and Ag with monolayer acceptor coverage. Substantial deviations are, however, found for Br-PyT/Ag(111) and NO_2-PyT/Ag(111), where in the latter case an adsorption-induced work function increase of as much as 1.6 eV is observed. This behavior is explained as arising from a face-on to edge-on reorientation of molecules in the monolayer. Our calculations show that for an edge-on orientation much larger work-function changes can be expected despite the prevalence of Fermi-level pinning. This is primarily ascribed to a change of the electron affinity of the adsorbate layer that results from a change of the molecular orientation. This work provides a comprehensive understanding of how changing the molecular electron affinity as well as the adsorbate structure impacts the electronic properties of electrodes.

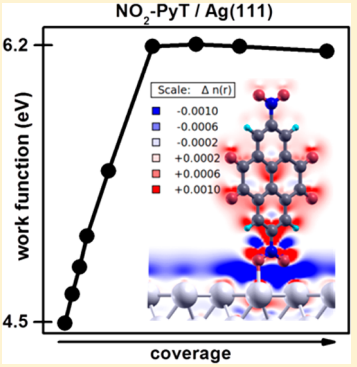

I. INTRODUCTION

Organic electronics has received considerable attention in the past three decades, and much effort has been spent on investigating and improving devices based on conjugated organic materials (COMs). The performance of organic electronic devices, like organic light-emitting diodes (OLEDs), photovoltaic cells (OPVCs), or field effect transistors (OFETs), is strongly affected by the interfaces between electrodes (metals, transparent conductive oxides, and conductive polymers) and the active COM layers.[1−4] Importantly, these interfaces can become bottlenecks for charge carrier injection when the energy difference between the frontier energy levels of the COM and the electrodes is large. Various methods have been developed to minimize charge injection barriers, such as the deposition of molecular interlayers that form polar bonds with the electrode,[5,6] the growth of thin interlayers of high work function metal oxides,[7] and the deposition of self-assembled monolayers comprising

Received: August 24, 2017
Revised: October 10, 2017
Published: October 27, 2017

intrinsic dipoles.[8−10] In all cases, an interfacial dipole layer is formed that changes the energy-level alignment and, thus, the hole- and electron-injection barriers (HIBs and EIBs).[11] A striking example is the molecular interlayer of the electron acceptor 2,3,5,6-tetrafluoro-7,7,8,8-tetracyanoquinodimethane (F4-TCNQ) that reduces the HIB for *p*-sexiphenyl (6P) on a gold electrode by up to 1.2 eV.[12] In general, the magnitude of the HIB decrease is related to the electron affinity (EA) of the acceptor.[13] However, the EA is only one of many factors, as the complex mechanism of interfacial electronic interaction includes electron donation and back-donation between the substrate and the adsorbate and involves, in addition to the frontier energy levels, also deep-lying levels.[14,15] A further beneficial mechanism for molecular interface modification is surface-induced aromatic stabilization (SIAS) of an organic molecule upon bond formation with the metal electrode,[16] and the proposed mechanism for SIAS is shown in Figure 1.

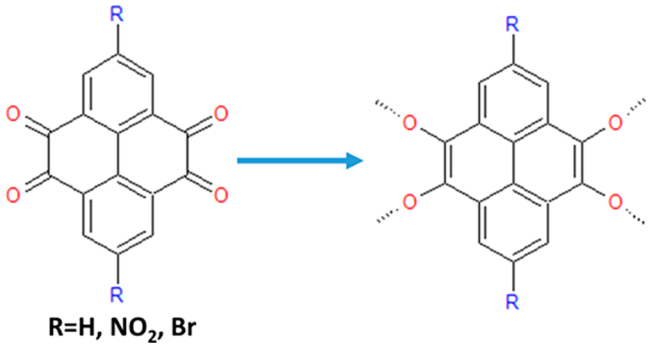

Figure 1. Chemical structures of pyrene-tetraone and its derivatives (left) and their structures upon SIAS after reaction with the metal surface (right).

Moreover, adsorption-induced changes of the molecular conformation can create intramolecular dipoles,[17] and molecular reorientation in the monolayer[18,19] can further impact interface energetics.[20,21] Therefore, work function changes by molecular monolayer adsorption cannot be readily predicted by simple models,[13,22] and although charge-injection-controlling interlayers are already successfully used in devices, further fundamental research on model substrates is necessary to get a complete picture of energetics at strongly coupled organic−inorganic interfaces.

In the present contribution, we provide insight into the impact of molecular orientation and electron affinity of electron acceptors in monolayers on a metal substrate. To that end, we investigated pyrene-4,5,9,10-tetraone (PyT) and two of its derivatives with electron-withdrawing functional groups, i.e., 2,7-nitro (NO_2-PyT) and 2,7-bromo (Br-PyT) (chemical structures in Figure 1), which offer the additional possibility of reorientation on the surface.[20] The PyT backbone is promising because it is an ideal candidate for exploiting SIAS[16,23] in order to increase its acceptor strength:[24] For the isolated (nonadsorbed) molecule, the carbonyl bonds break the conjugation of the pyrene core. Upon adsorption on the surface, however, the bond order of the C═O bonds is reduced allowing the core to adopt a more pronounced aromatic structure. Moreover, carbonyl groups play a pivotal role in surface catalysis.[25,26] Apart from its potential application in electrode work function tuning,[27,28] PyT and its derivatives have attracted attention both in battery[29,30] and in sensor developments.[31] In the present contribution, we study the title compounds deposited on Au(111) and Ag(111) by ultraviolet and X-ray photoelectron spectroscopy (UPS, XPS) and the X-ray standing wave (XSW) technique,[32,33] complemented by density functional theory (DFT) calculations.

II. EXPERIMENTAL AND COMPUTATIONAL DETAILS

Experimental Methods. The pyrene-based molecular acceptors were synthesized according to ref 34. The metal single crystals were cleaned by repeated cycles of annealing (up to 550 °C) and Ar-ion sputtering. Afterward, the organic acceptor molecules were sublimed onto the clean surfaces from resistively heated sources. The nominal mass−thickness of the organic layers was monitored with a quartz crystal microbalance. During COM deposition as well as during UPS, XPS, and XSW measurements the samples were kept at room temperature. UPS and XPS were performed at the endstation SurICat (beamline PM4) at the synchrotron light source BESSY II (Berlin, Germany).[35] Spectra were collected with a hemispherical electron energy analyzer (Scienta SES 100) using an excitation photon energy of 35 eV for UPS and 650 eV for XPS. The secondary electron cutoff (SECO) spectra were obtained with the samples biased at −10 V. The error of energy values reported here is estimated to be ±0.05 eV. The experimental setup consists of interconnected sample preparation (base pressure $<7 \times 10^{-9}$ mbar) and analysis (base pressure 1×10^{-10} mbar) chambers, which enables sample transfer without breaking vacuum conditions. Binding energy (BE) values are reported relative to the Fermi level of the clean metal crystals. The XSW experiments were done in back reflection geometry at beamline ID32 at the ESRF (Grenoble, France).[36] The submonolayer PyT and NO_2-PyT coverage was confirmed by the evaluation of C 1s and Ag 3d photoemission intensities. PyT was measured in the "XSW chamber" of the ID32 endstation (base pressure 3×10^{-10} mbar) with the electron analyzer mounted at an angle of 45° relative to the incoming X-ray beam, while NO_2-PyT was studied in the "HAXPES chamber" (base pressure 2×10^{-10} mbar) with a photoelectron emission angle close to 90°. The analysis of the XSW data was done using the software package *dare* (developed at the ESRF). The errors of the average bonding distances are estimated as ±0.05 Å. The non-dipole contributions to photoemission spectra collected at an emission angle of 45° were corrected according to refs 37 and 38. Core-level spectra (in the XSW as well as the XPS analysis) were fitted with Voigt profiles using the *Winspec* software package (University of Namur, Belgium). For NO_2-PyT the carbonyl and the nitro oxygen species have been fitted separately. In the fitting process for the coherent positions and fractions, the latter depend critically on external parameters like the substrate's mosaicity, the experimental geometry, or noise in the data. Thus, the coherent fractions measured for NO_2-PyT and PyT, respectively, cannot be directly compared. The coherent positions, however, are robust and do not depend critically on the experimental conditions.

Computational Methods. DFT-based band structure calculations in the repeated-slab approach were carried out using FHI-aims[39] employing the Perdew−Burke−Ernzerhof (PBE)[40] generalized gradient approximation (GGA). Van der Waals (vdW) forces were accounted for through the vdW-TS scheme,[41] parametrized for molecules on surfaces.[42] The application of GGA functionals suffers from methodological deficiencies, in particular the self-interaction error[43,44] and the missing band gap renormalization at the interface.[45−47]

DOI: 10.1021/acs.jpcc.7b08451
J. Phys. Chem. C 2017, 121, 24657−24668

However, it has been shown that for molecules that hybridize with the metal surface, such as in the present case, the adsorption-induced work function modifications are generally appropriately described using PBE[48] and that employing hybrid functionals does not improve the situation significantly.[49] FHI-aims' "tight" basis set defaults have been used throughout, except for an increase of the cutoff potential of Ag to 4.0 Å. To facilitate the numerical convergence, a Gaussian broadening of 0.1 eV has been employed.

PyT and its derivatives were put onto 5-layer slabs of Ag or Au, with a >20 Å vacuum gap separating periodic replicas of the slab in z-direction; a self-consistently determined dipole layer[50] in the vacuum was used to electrostatically decouple the periodic replicas. All atoms of the molecules as well as the top two metal layers were fully relaxed using a damped molecular dynamics scheme until all remaining forces were below 0.01 eV/Å. All calculations were done in a non-spin-polarized manner. To allow for a systematic comparison, a $(3\sqrt{3} \times 5)$ unit cell as previously used in theoretical studies of F4-TCNQ on metal surfaces[15,48] was assumed for all systems. This unit cell was kept also for studying the upright-standing model system to show the impact of molecular reorientation. In this way, the obtained results are not additionally impacted by the expected higher packing density for an upright-standing phase. As the latter would very likely increase the molecular dipole density, the calculated work-function change for the low-density upright-standing phase represents a lower limit for what is to be expected in the actual film (see also discussion at the end of section III).

All geometries and the results of the final calculations have been uploaded to the NOMAD database (www.nomad-repository.eu) and are downloadable as a data set under the doi: http://dx.doi.org/10.17172/NOMAD/2017.06.23-1.

3D representations of the interface structures were produced using XCrysDen.[51]

III. EXPERIMENTAL AND COMPUTATIONAL RESULTS

Impact of Electron-Withdrawing Substituents. The expected metal−molecule charge transfer and the concomitant work function change crucially depend on the electron affinity of the adsorbed molecules. Therefore, in our study we assess the impact of the NO_2 and Br substituents on the molecular oxidation potential, done by cyclovoltammetry (CV) (Figure S1). Therefrom, we determine the electron affinity (EA) of PyT to be 4.0 eV and find slightly higher values (4.2 and 4.3 eV) for the Br- and NO_2-substituted derivatives, respectively. Naively, one could, therefore, expect that the work function change induced by all three molecules is the same within 0.3 eV. However, as shown in the following, this assumption is not always fulfilled.

Photoelectron Spectroscopy of PyT and Its Derivatives on Au(111) and Ag(111). Turning toward the solid state, we start with the adsorption of the acceptors on Au, the less reactive metal compared to Ag. The evolution of the work function, as measured by UPS, is shown in Figure 2 as a function of molecule coverage. For all three acceptors, we can distinguish between a low-coverage and a high-coverage region: At low nominal coverage, i.e., up to $\theta \approx 6$ Å, we find a strong reduction of the pristine Au work function from $\phi = 5.45$ eV to 4.75 eV for PyT, 5.15 eV for NO_2-PyT, and 4.95 eV for Br-PyT. At higher coverage, i.e., up to $\theta \approx 100$ Å, the work function remains essentially constant for PyT and NO_2-PyT, while for Br-Pyt a further slight, roughly linear further work function

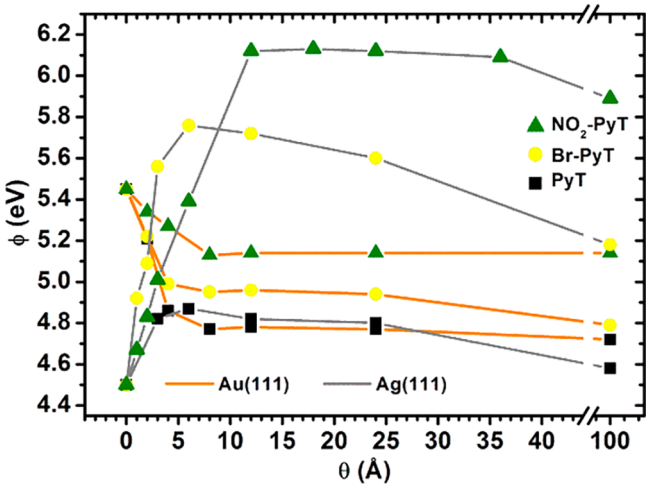

Figure 2. Work function (ϕ) as a function of nominal coverage (θ) of the PyT derivatives on Au(111) and Ag(111), respectively. The error bar of all data points is ±0.05 eV.

reduction is observed. On the basis of these data, we ascribe the evoluation at low-coverage region to the formation of the first monolayer and higher coverage to multilayer formation. In general, the decrease in ϕ upon the deposition of all three acceptors on Au(111) points to a comparably weak interaction with the substrate. The magnitude of the overall workfunction decrease ($\Delta\phi$) for PyT on Au(111) is −0.70 eV and thus in the typical range found for physisorbed molecules on Au, where the push-back effect, i.e., the repulsion between the molecular and metal electron density, is the main origin of this work-function change.[52,53] The smaller $\Delta\phi$ for NO_2-PyT and Br-PyT can be explained by a larger adsorption distance due to the more bulky side groups that reduce the push-back effect.[54] This is supported by simulations, which are discussed below. An alternative scenario to explain the work-function evolution would be (very small) electron transfer from the metal to the adsorbate or a combination of both effects. In any case, the spread of the observed work function modifications is only slightly larger than the 0.3 eV difference of the EA values obtained from CV.

The situation is markedly different for Ag(111), as shown in Figure 2. For all three acceptor molecules, we find two qualitatively different regimes. The low coverage regime is characterized by a pronounced *increase* of the work function from 4.50 eV for pristine Ag(111) to 4.85 eV (PyT, $\theta \approx 6$ Å), 6.15 eV (NO_2-PyT, $\theta \approx 12$ Å), and 5.75 eV (Br-PyT, $\theta \approx 6$ Å). At higher coverage (up to 100 Å) all three interfaces show a gradual decrease of the work function. Noteworthy, the differences between the measured work function changes (1.3 eV) are now *significantly larger* than the differences of the molecular EAs obtained from CV (0.3 eV).

The increase in ϕ on Ag(111) by the adsorbed acceptors points to a charge transfer reaction involving a net electron transfer from Ag to the adsorbate. The increase in work function for NO_2-PyT by 1.60 eV is significantly larger than that induced by F4-TCNQ on Ag(111) ($\Delta\phi < 0.70$ eV)[48,55] and shows the high potential of this acceptor for achieving high ϕ electrodes. The maximum ϕ for NO_2-PyT is reached for a nominal layer thickness of 12 Å (i.e., twice the value of the other two compounds). Assuming flat-lying molecules, which is a typical adsorption geometry for similar acceptors on clean metal surfaces[11,56,57] (and is evidenced for submonolayer

DOI: 10.1021/acs.jpcc.7b08451
J. Phys. Chem. C 2017, 121, 24657−24668

coverage by XSW, see below), this corresponds to significantly more than monolayer coverage, which, therefore, would indicate metal−organic charge transfer beyond the monolayer. A more realistic scenario would be that the 12 Å film corresponds to an edge-on oriented monolayer; i.e., that we witness an orientational transition of the initially flat-lying NO_2-PyT monolayer. Such a transient monolayer structure has already been observed for hexaazatriphenylene-hexacarbonitrile (HATCN) on Ag(111),resulting in an increase of the work function by 1.0 eV.[20]

The qualitative differences between adsorption on Au(111) and Ag(111) are also clearly seen in the UPS valence band (VB) spectra for PyT and NO_2-PyT (see Figures 3 and 4). At

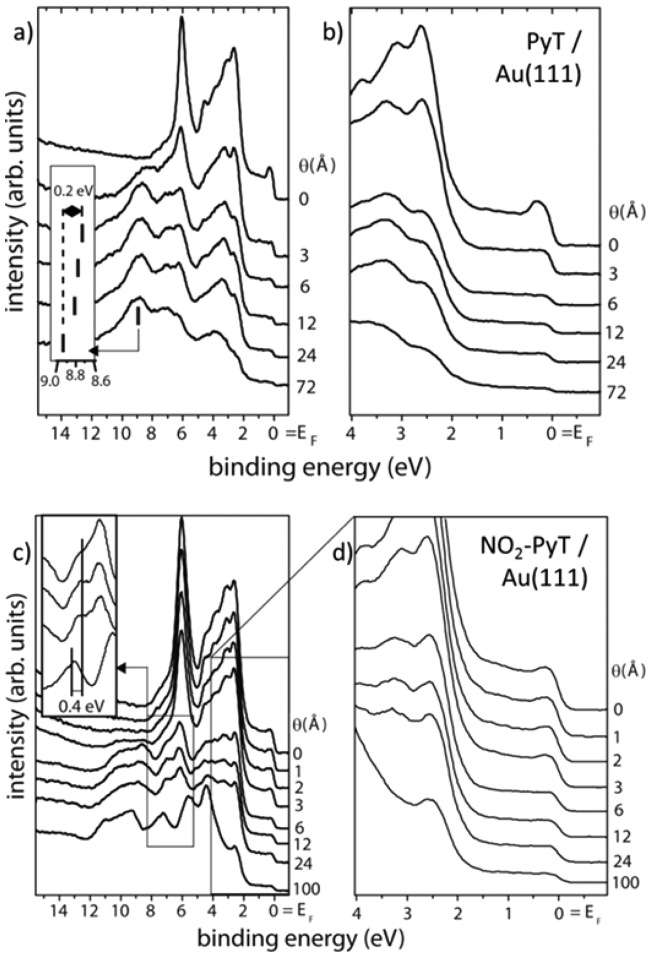

Figure 3. UPS valence spectra of sequentially deposited PyT (a, b) and NO_2−PyT (c, d) on Au(111); the nominal coverage is denoted by θ. (a, c) Full UPS valence band spectrum and (b, d) zoom into the region near Fermi-level (E_F) region; the insets depict the shift of the peak position of a PyT molecular level in more detail.

low coverage, for PyT and NO_2-PyT on Au(111) (Figure 3), we can clearly identify characteristic substrate features (the metal Fermi edge, the Shockley surface state, d-bands in the region between 2 and 7 eV below E_F), which strongly decrease in intensity with increasing θ. The metal Fermi edge remains visible even at the highest nominal coverage of 100 Å. This is strong evidence for island or Stranski−Krastanov (island on wetting layer) growth. Upon increasing coverage, also several molecule-derived features become clearly visible at binding energies ≥2 eV. Importantly, no additional features emerge

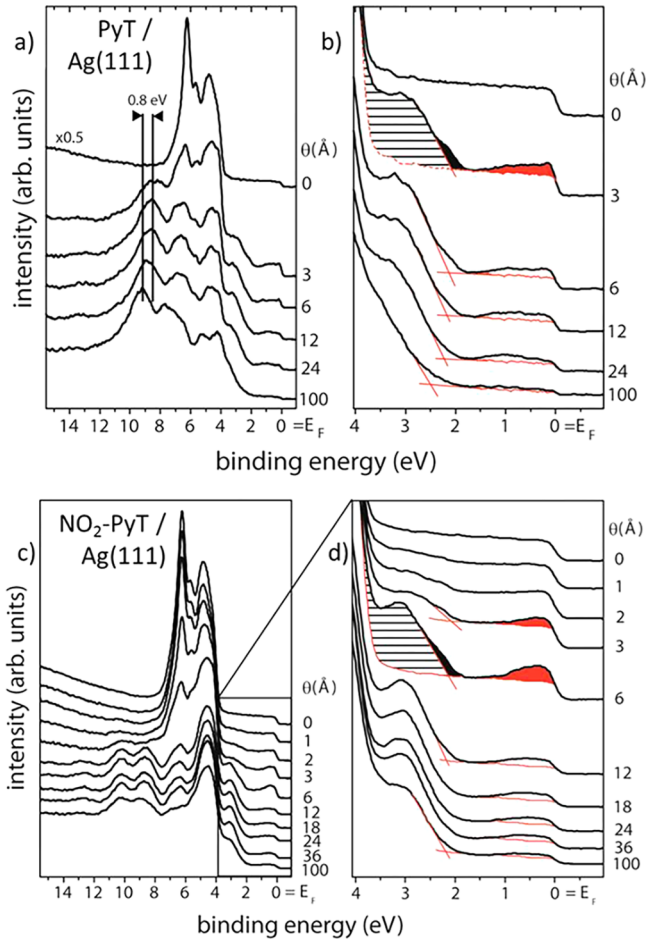

Figure 4. UPS valence spectra of sequentially deposited PyT (a, b) and NO_2-PyT (c, d) on Ag(111). The nominal coverage is denoted by θ. (a, c) Full UPS valence band spectrum and (b, d) zoom into the near-Fermi-energy region. E_F denotes the Fermi level. The filled areas in b and d denote the approximate spectral contributions from organic/metal hybrid states and the anion species of PyT (NO_2-PyT) determined by using the spectrum of pristine Ag(111) as the boundary.

close to the Fermi level (E_F). Their appearance would point toward substantial electron transfer to the molecule.[12,16] Conversely, their absence indicates that no (significant) charge transfer occurs these systems. A close inspection of Figure 3a reveals a shift of the PyT-derived peak at ca. 8.8 eV to higher binding energy (by ca. 0.2 eV) with increasing coverage (inset in Figure 3a). This shift is small compared to typical chemical shifts and rather attributed to a decreased final state screening for molecules farther from the metal.[57,58] Note that also the C 1s and O 1s core levels (Figure S2) show similar coverage-dependent shifts. This points to weak, i.e., nonchemisorptive interaction, indicating that SIAS is not occurring here.

In contrast to the situation on Au(111), the adsorption for PyT and equally for NO_2-PyT on Ag(111) (Figure 4) produces molecular-derived states close to E_F (red area in Figure 4b). Concomitantly, another distinctive broad feature at ∼3.0 eV BE (shaded area) and a shoulder at its low BE side (black area) appear. All three features show their maximum intensity between 3 and 6 Å coverage, which indicates that they originate from molecules in the interfacial region. The occurrence of the new peaks is reminiscent of what was observed for related acceptors on metal surfaces, e.g., F4-

DOI: 10.1021/acs.jpcc.7b08451
J. Phys. Chem. C 2017, 121, 24657−24668

TCNQ,[12] HATCN,[59] 3,4,9,10-perylenetetracarboxylic-dianhydride (PTCDA),[17,60] perylene-3,4,9,10-tetracarboxylic diimide,[61] 6,13-pentacenequinone (P2O), 5,7,12,14-pentacenetetrone (P4O),[16] and diindenoperylene (DIP),[62,63] where substantial negative charge is transferred from the substrate to the molecule upon chemisorption. In analogy, we assign the feature close to the Fermi level to hybrid orbital(s) formed by metal states and the molecular LUMO now being partially filled. The feature at ~2 eV BE (also extending into the shaded region at higher BE) is associated with the former HOMO of PyT (now also involved in hybridization with metal states and relaxed in energy). The broad peak at ~3 eV BE as well as that at ~8.4 eV BE also originate from PyT bound to the metal. The latter peak exhibits an apparent shift to higher BE (0.8 eV) with increasing coverage. This is much larger than the corresponding shift on Au and cannot be explained by screening alone.[57,58] Furthermore, in the C 1s core-level spectra of PyT on Ag(111) the strong chemical shift between aromatic carbon and carbon bound to oxygen is observed for multilayer coverage only but not for molecules in direct contact with the substrate (Figure S3). This observation is consistent with SIAS, where all carbon atoms become aromatic.[16]

The VB spectra of NO_2-PyT on Ag(111) (Figures 4c and 4d) and the respective core-level spectra (Figure S3) are almost identical to those of PyT/Ag(111) pointing toward similar mechanisms. Core-level spectra of Br-PyT on Ag(111) (Figure S5) strongly suggest (partial) C−Br bond cleavage. However, from the large work function increase (up to 1.3 eV, Figure 1) upon deposition of Br-Pyt on Ag(111) and from the evolution of valence spectra (Figure S7) we conclude that also Br-Pyt undergoes pronounced charge transfer on the Ag(111) surface.

Bonding Distances of PyT/Ag(111) and NO_2-PyT/Ag(111) Determined by the X-ray Standing Wave Technique. The similarity of the valence spectra of the PyT/Ag(111) and NO_2−PyT/Ag(111) interfaces raises the question why the maximum work-function modification for the two adsorbates differ by more than 1 eV. A pronounced dependence of the work function change on the details of the adsorbate geometry (i.e., the molecular orientation or out-of-plane distortion) has been repeatedly discussed.[64−66] To assess the role of the bonding distances and possible molecular distortions, we thus performed XSW experiments.[67,68] For organic monolayers on single-crystal metal substrates, XSW can access vertical adsorption distances with high precision by measuring the photoelectron yield (Y_p) of adsorbate atoms as a function of the X-ray photon energy E.[33,69] Figure 5 displays the least mean square fits of Y_p's, which give the coherent positions P_H and the coherent fractions f_H. The former provide the average bonding distance d_H in terms of the lattice plane spacing d_0 of the (111) Bragg reflection of the substrate via $d_H = (n + P_H)d_0$ (with n being a non-negative integer). The coherent fraction reflects the degree of vertical order of the adsorbate atoms and is 0 for total disorder and 1 for perfect order (i.e., the hypothetical case where all adsorbate atoms have identical bonding distance).

The XSW measurements for PyT submonolayers on Ag(111) (Figure 5a) yield average bonding distances of 2.46 Å for the carbon and 2.31 Å for the oxygen atoms; i.e., the oxygen atoms are found significantly closer to the substrate. The values are summarized in Table 1. Note that the averaged Ag−C distance is much shorter than for weakly interacting monolayers on the same substrate, e.g., DIP (3.01 Å),[70] 7,8,15,16-tetraazaterrylene (2.99 Å),[71] pentacene (2.98 Å to 3.12 Å),[72] or P2O (3.32 Å).[16] Moreover, also strongly interacting systems like P4O (2.69 Å) or PTCDA (2.81 Å to 2.86 Å)[38,73,74] have longer averaged Ag−C bonding distances, and the difference between averaged carbon and oxygen distances (0.15 Å) is smaller than that of P4O/Ag(111) (0.26 Å).[16] The low coherent fraction measured for the C atoms points to a bent carbon skeleton.[56,69] The short bonding distances and the bent conformation are a further clear indication of strong PyT/Ag interaction.

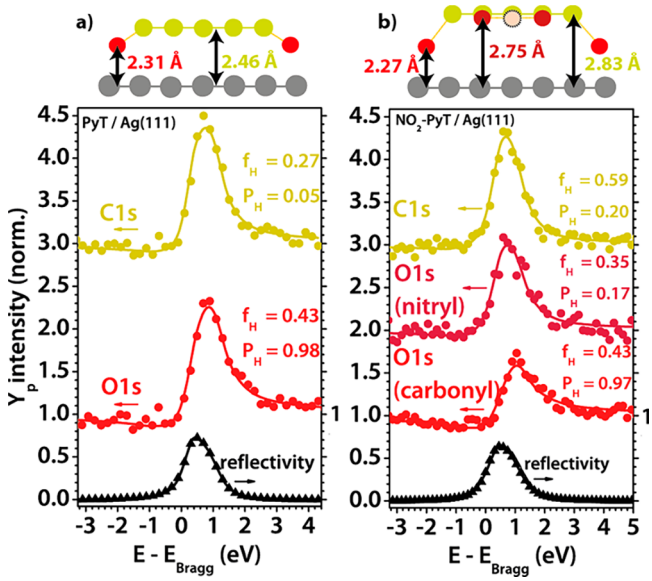

Figure 5. Sketch of experimental bonding distances of (a) PyT and (b) NO_2-PyT in submonolayers on Ag(111) obtained by a least mean square fit of the photoelectron yield (Y_p) of the carbon and the oxygen, respectively, which is plotted together with the reflectivity as a function of photon energy minus Bragg energy (E_{Bragg} = 2.63 keV). f_H denotes the coherent fraction and P_H the coherent position.

The averaged Ag−C distance for NO_2-PyT on Ag(111) is 2.83 Å and thus much longer than for PyT on the same substrate. Unfortunately, an experimental determination of bonding distances of nitrogen atoms on Ag(111) was not possible, as the N 1s signal too strongly overlaps with a Ag 3d plasmon.[71] Nevertheless, the position of the $-NO_2$ group could be determined relying on the substantial chemical shift between carbonyl and nitro O 1s levels. Following ref 38 we fitted each of the two O 1s components with a separate peak and used its area as input for the photoelectron yield in the further analysis. The oxygen atoms of the nitro groups are located significantly above the carbonyl-oxygen atoms, however, still below the carbon atom average, at a distance of 2.75 Å. Hence, there is essentially no vertical dipole introduced by the $-NO_2$ groups that could explain the extraordinarily large work function increase observed for NO_2-PyT. Comparing PyT to NO_2-Pyt, the carbonyl oxygen atoms show almost the same bonding distance on Ag(111) (2.27 Å). The distance of the carbon skeleton is, however, increased by ca. 0.4 Å, which we attribute to the bulky NO_2 groups.

Density Functional Theory Modeling. Having established that PyT and its derivatives adopt a flat-lying conformation in the submonolayer, we turn to first-principles modeling via dispersion-corrected density-functional-theory based band-structure calculations. This yields complementary information on the impact of functional side groups on the electronic structure and allows us to gain fully atomistic insight.

DOI: 10.1021/acs.jpcc.7b08451
J. Phys. Chem. C 2017, 121, 24657−24668

Table 1. Experimental and Calculated Monolayer Bonding Distances (d_H) of PyT and NO_2-PyT on Ag(111) Derived from XSW Measurements (Submonolayer Coverage) and DFT Simulations[a]

		carbon		carbonyl oxygen		nitro oxygen	
		d_H (Å)	f_H	d_H (Å)	f_H	d_H (Å)	f_H
measured	PyT/Ag(111)	2.46	0.27	2.31	0.43		
calculated		2.56−2.92 (2.37−2.76)		2.26−2.34 (2.01−2.06)			
measured	NO_2-PyT/Ag(111)	2.83	0.59	2.27	0.43	2.75	0.35
calculated		2.60−2.90 (2.38−2.69)		2.32−2.39 (2.02−2.09)		2.51−2.66 (2.31−2.45)	

[a]Simulated results are given for a full optimization of the molecule without relaxation of the Ag lattice (i.e., neglecting surface relaxations). The distances after including the relaxation of the topmost layers, but reported with respect to the hypothetical, unrelaxed Ag surface, are given in brackets. These values are consistent with the actually measured quantities. For experimental results, also the respective coherent fractions (f_H) are given.

Figure 6a shows the calculated projected density of states (PDOS) of the three acceptors on Au(111). In all cases, the Fermi level cuts through the low-energy tail of the LUMO-derived feature. This implies that all molecules are at the onset of Fermi-level pinning; i.e., the work function of the combined systems is determined by the electron affinities of the adsorbate layers. However, substrate-to-adsorbate electron transfer is likely too small to be clearly observable in the UPS valence spectra. This explains why the observed trend in work functions correlates so well with that of the molecular electron affinities. In this context, it is noteworthy that calculated and measured work function values agree very well for all three molecules adsorbed on Au(111) (see Table 2).

Quantifying charge transfer is always ambiguous since the "molecular charge" is not a physical observable *per se*. This is particularly problematic in the current case, as charge transfer is small and different charge-partition schemes can yield even qualitatively different results. Therefore, we rely on the real-space redistribution of electron density. In particular, we calculate the real-space charge rearrangements $\Delta\rho$ as

$$\Delta\rho = \rho^{sys} - (\rho^{slab} + \rho^{ML}) \quad (1)$$

where ρ^{sys} is the electron density of the combined system; ρ^{slab} is the electron density of the metal slab without the adsorbate; and ρ^{ML} is the electron density of a hypothetical, free-standing monolayer of the adsorbate. From $\Delta\rho$, one can obtain the cumulative charge transfer function Q by integrating from infinity to the position of a plane z

$$Q(z) = \int_{-\infty}^{z} \Delta\rho dz \quad (2)$$

Q yields the amount of total charge that is transferred from above to below a plane at position z as a consequence of the adsorption of the molecule. The maximum absolute value of Q can serve as a measure for the net charge transfer between substrate and adsorbate.

Figure 6b shows the charge rearrangements, $\Delta\rho$, for the PyT derivatives on Au(111) as a function of position above the substrate. For PyT and Br-PyT, Q (shown in Figure 6c) is positive at essentially all distances. This indicates a net shift of electron density toward the substrate, fully consistent with Pauli push-back.[6] Moreover, this also correlates well with $\Delta\rho$, where we observe a pronounced increase in electron density within and directly above the substrate. In contrast, for NO_2-Pyt, the evolution of the cumulative charge-transfer function displays a qualitatively different shape with a pronounced peak between the substrate and the adsorbate backbone. This is indicative of transfer of electrons into a molecular π-orbital (i.e., its LUMO). Here, this dominates over Pauli push-back in terms of contribution to ϕ. We attribute this observation to a combination of two effects: On the one hand, the increased distances of NO_2-PyT lead to a reduction of the push-back effect compared to the other two molecules. On the other hand, the higher EA also leads to a larger electron transfer into the molecule.

On Ag(111), the DFT calculated geometries are consistent with the XSW measurements, showing PyT to adopt a bent conformation. In good agreement with the experimental values, the carbon atoms are found at distances between 2.56 and 2.92 Å and the oxygen atoms at distances between 2.26 and 2.34 Å from the uppermost metal atoms (see Table 1). Such an agreement for the adsorption distances is a prerequisite for obtaining a meaningful electronic structure in the calculations.[15] Indeed, the calculated work function of 4.61 eV for the PyT covered Ag(111) surface is in good agreement with the measured 4.85 eV (Figure 2).

On Ag(111), the filling of the LUMO-derived band is much more pronounced than on Au(111), as can be seen in the calculated PDOS of PyT and its derivatives (Figure 7a). This is the reason why on this lower work function substrate the electron transfer to the adsorbate layer is unmistakably observed in the experiments (see Figure 4). The accumulation of the electron density is clearly seen in the charge rearrangements shown in Figure 7 b and c: All three molecules accept electrons from the surface with an increasing net transfer from PyT (0.45 electrons) to Br-PyT (0.50 electrons) and to face-on NO_2-PyT (0.71 electrons).

In passing, we note that on top of the charge transfer related dipole there is also a dipole caused by the bent-down carboxylic oxygens with the net effect causing the adsorption-induced work function change. All individual dipoles have to act such that the final work function eventually corresponds to the electron affinity of the adsorbate layer. As discussed in detail in ref 64, this is a consequence of the Fermi level pinning situation and the fact that none of the molecular dipoles resides above the molecular backbone, where the LUMO is localized. This also explains why for PyT/Ag(111) and PyT/Au(111) very similar work function values are obtained in the simulations and in the experiments.

Concomitantly, in the simulations for Br-PyT/Ag(111) and NO_2-PyT/Ag(111) the calculated work functions increase also on Ag(111) only slightly compared to PyT/Ag(111) analogous to the observations on Au(111). This, however, results in calculated work function changes for Br-PyT/Ag(111) and NO_2-PyT/Ag(111) significantly smaller than those observed experimentally. This points toward a fundamental difference between the situation in the experiment and that assumed for the modeling (i.e., a monolayer of molecules lying flat on the

DOI: 10.1021/acs.jpcc.7b08451
J. Phys. Chem. C 2017, 121, 24657−24668

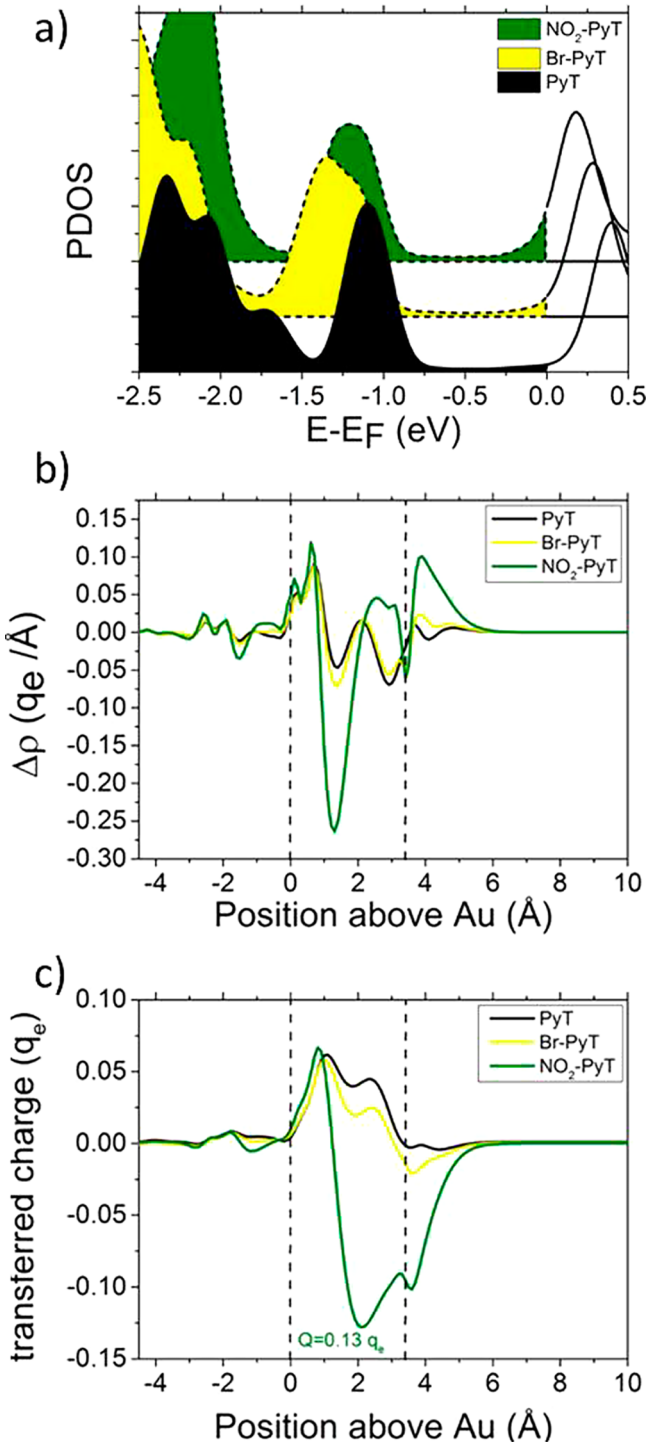

Figure 6. PyT, Br-PyT, and NO_2-PyT adsorbed on Au(111). (a) Projected density of states (PDOS) for the three molecules adsorbed on Au(111). The PDOSs are offset for clarity. (b) Adsorption-induced charge rearrangements $\Delta\rho$ (as defined in eq 1) for the three molecules. (c) Cumulative charge transfer (as defined in eq 2) for the three molecules adsorbed on Au(111). The averaged position of the carbon atoms and the topmost Au plane are indicated by vertical lines. q_e represents the charge of an electron.

surface). In the discussion of the experimental work function trends, charge transfer beyond the first adsorbate layer has been suggested as one possible origin for the large work functions experimentally obtained for NO_2-PyT/Ag(111) (vide supra). This would, indeed, be consistent with the observation that at

Table 2. Measured and Calculated Work Functions of the PyT Derivatives on Au(111) and Ag(111), Respectively[a]

		substrate	PyT	Br-PyT	NO_2-PyT
measured	Au(111)	5.45	4.75	4.95	5.15
calculated		5.16	5.04	5.02	5.22
measured	Ag(111)	4.50	4.85	5.75[b]	6.15[b]
calculated		4.45	4.61	4.67[b]	4.97 (5.71)[b]

[a]The measured values are derived from the SECOs for a nominal coverage of 12 Å. DFT simulations have been performed for a coverage of one molecule in a $5 \times 3\sqrt{3}$ unit cell; all values given in eV. [b]As discussed in the main text, for those two cases in the experiments nonflat-lying adsorption configurations are expected at variance with the structures considered in the simulations. Thus, for the NO_2-PyT case, a second calculated value for a (low-coverage) conformation with upright-standing molecules is included.

coverages up to the monolayer region the evolutions for PyT and NO_2-PyT are nearly the same. In particular at a nominal coverage of 4 Å $\Delta\phi$ is only 0.2 eV larger for NO_2-PyT than for PyT and thus in quantitative agreement with the simulations of the flat-lying monolayer.

The key difference between the two systems is that, while $\Delta\phi$ saturates for PyT at 6 Å, for NO_2-PyT the maximum work function change occurs at a nominal coverage of 12 Å. In this view, the maximum work function of ϕ = 6.15 eV at 12 Å would then correspond to the situation of at least two essentially flat-lying layers with charge transfer also to the second one. A problem with this explanation is that for a Fermi-level pinned adsorbate layer, work functions significantly exceeding the molecular electron affinity are only expected in situations where dipole moments are located above the region in which the orbital responsible for the pinning is localized. This is, however, not the case for the (essentially) flat-lying layers here.[64]

Such a situation could, however, be encountered for edge-on molecules at 12 Å nominal thickness. In general, the bonding distances in monolayers of edge-on molecules cannot be determined with XSW as the adsorbate atoms cover a wide range of bonding distances, which reduces the coherent fraction to zero.[56] Thus, to test that hypothesis, we calculated the situation for an upright-standing geometry of NO_2-PyT. We emphasize at this point that changing the coverage would increase the work function for any arbitrary geometry. Indeed, by changing the coverage, it would be possible to reproduce (almost) any experimental value. In order to avoid producing a "right" result for the wrong reason, we therefore restricted the calculations to one upright standing molecule per $(3\sqrt{3} \times 5)$ unit cell, i.e., to a situation with the same coverage as in the lying down situation. As expected, this results in a significantly amplified work-function increase to 5.71 eV ($\Delta\phi$ = 1.26 eV). The absolute value is still smaller than observed experimentally, but this is merely attributed to the comparably low coverage in the simulations. Indeed, upon increasing the coverage of upright-standing molecules a significant further increase of the work function can be expected, as has been seen, for example, for the HATCN/Ag(111) interface.[20]

Furthermore, it should be stressed that a significant increase of $\Delta\phi$ could also be obtained for other adsorption geometries, such as a geometry which binds via two of the four carboxyl groups. Ideally, we would like to determine the energetically most favorable structure, especially around the coverage where the reorientation occurs. Although methods to determine monolayer structures at interfaces are currently under active

DOI: 10.1021/acs.jpcc.7b08451
J. Phys. Chem. C 2017, 121, 24657−24668

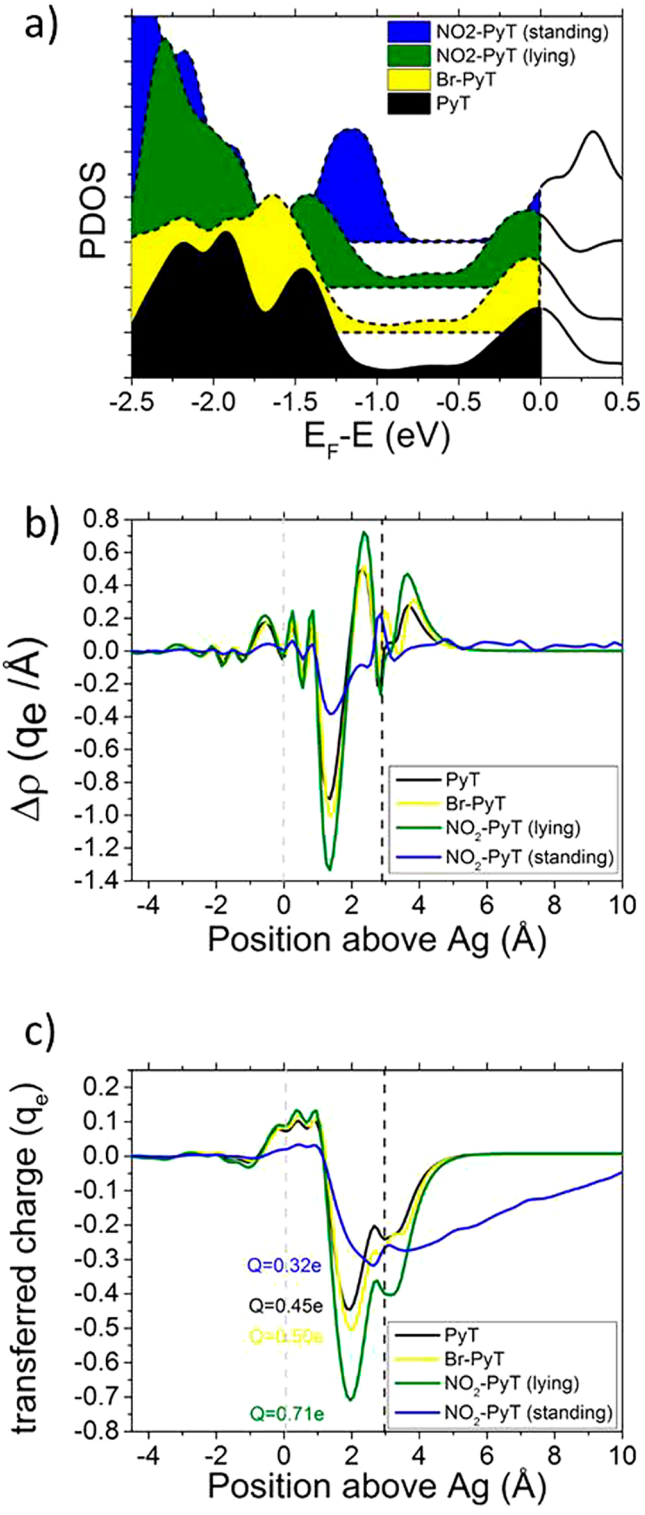

Figure 7. PyT, Br-PyT, and NO_2-PyT adsorbed on Ag(111) for NO_2-PyT results for face-on (lying) and edge-on (standing) orientations are displayed. (a) Projected density of states (PDOS). (b) Adsorption-induced charge rearrangements $\Delta\rho$. (c) Cumulative charge transfer. The averaged position of the carbon atoms (for lying molecules) and the topmost Ag plane are indicated by vertical dashed lines.

development,[75−77] without experimental input on the size or the shape of the unit cell, or the precise coverage, they presently remain too expensive to be performed on a routine basis. For this reason, it is important to understand the origin of the observed large work-function shift in more detail. As we will show in the following, only for an upright-standing NO_2-PyT layer, work-function changes far beyond the expectation based on the molecular electron affinities are possible.

To understand that, it is first crucial to realize that Fermi-level pinning prevails for the upright standing layer, as can be seen in the corresponding DOS included in Figure 7a. This notion is confirmed by the adsorption-induced charge rearrangements for the upright-standing NO_2-PyT layer. The corresponding isodensity plot is shown Figure 8, while plane-averaged charge rearrangements are contained in Figure 7b and c.

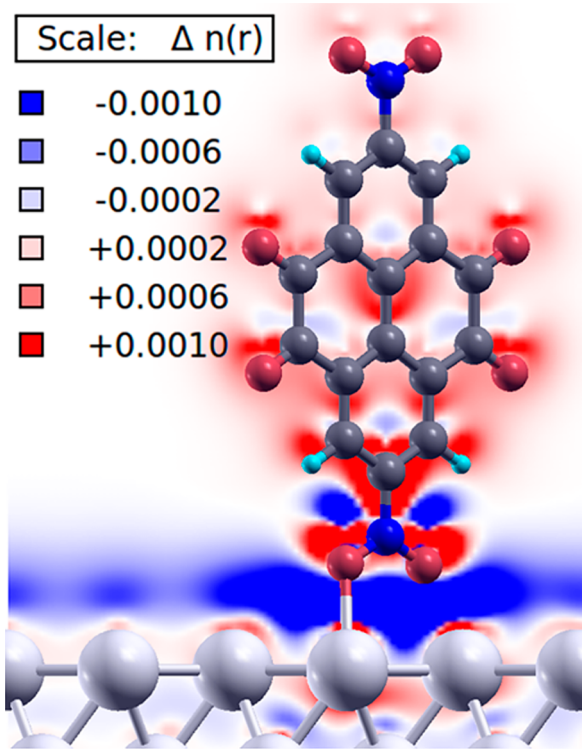

Figure 8. DFT-calculated adsorption-induced charge rearrangements for the adsorption of an upright standing NO_2-PyT monolayer, averaged in the direction perpendicular to the paper plane.

One can see that adsorption results in a charge accumulation, which is mostly localized in the bottom half of the molecule; the nodal structure of the charge rearrangements is reminiscent of the molecular LUMO of NO_2-PyT supporting the notion of Fermi-level pinning through a partial filling of hybrid states containing contributions of that orbital. This raises the question why pinning at LUMO-derived states causes work-function modifications that (in the calculations) are by more than 0.7 eV smaller for flat-lying molecules compared to upright-standing layers (with the trend being even more pronounced in the experiments).

To understand that, one has to keep in mind that in the case of Fermi-level pinning, in a first approximation, the electron affinity of the monolayer determines the sample work function.[13,78] This quantity is, however, strongly dependent on the orientation of the molecules within the monolayer due to the presence or absence of molecular dipoles at the periphery of that layer. The collective field from those dipoles then shifts the molecular states relative to the vacuum level, as some of us previously explained in detail.[79,80] In the present

DOI: 10.1021/acs.jpcc.7b08451
J. Phys. Chem. C 2017, 121, 24657−24668

case, this results in a difference in the positions of the LUMO-derived bands relative to the vacuum level of ∼0.4 eV between lying and standing monolayers (see Figure 9). This shift is primarily a consequence of the dipole moments of the $-NO_2$ groups, which only for upright-standing molecules lie between the π-backbones and the vacuum. Again, it should be stressed that their effect is not diminished by the dipoles of the $-NO_2$ groups between the molecules and the substrate (as one might assume on the basis of mere symmetry arguments). As discussed in detail in ref 64 for the case of Fermi-level pinning those "bottom" molecular dipoles have to be fully compensated by the interfacial charge rearrangements. The cruicial role of the local dipole moment also explains why it is more sensible to assume a geometry where the molecule stands on the NO_2 groups than on the C═O groups. In the latter case, the terminal group (H, Br, NO_2) for all X-PyT molecules would be parallel to the surface and therefore would not contribute to the work-function increase at all. Although one would still expect a strong work-function increase upon reorientation of the molecule (due to the dipole moment of the C═O group protruding into vacuum), the final work function should then be (almost) the same for all three molecules. This is, however, not seen in the experiments (see Figure 2). Therefore, only adsorption geometries where the z-component of the dipole moment of the terminal group remains nonzero are consistent with the experimental observations.

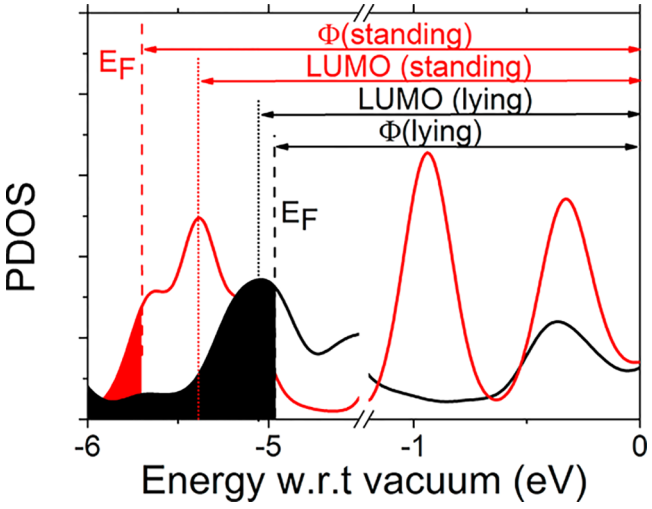

Figure 9. Densities of states calculated for standing and lying NO_2-PyT layers plotted relative to the vacuum level above the sample. The vertical dashed lines indicate the position of the Fermi level, while the dotted lines denote the maximum of the LUMO-derived feature in the DOS projected onto the monolayer. Data for the standing layer are plotted in red, while those for the lying layer are in black.

In order to understand how the reorientation affects the level alignment and, thus, the work function, it is important to remember that in Fermi-level pinned systems[81,82] the bond dipole between the substrate and adsorbate is always so large that it shifts the molecular state into resonance with the Fermi edge.[49] Molecular dipoles between the pinned state and the Fermi edge that would shift the molecular state to lower energies are therefore compensated by a large charge-transfer-induced dipole.[64] The large dipole, however, does not necessarily imply a larger transfer. Rather, it can also be realized by a larger distance over which the charge is transferred. Exactly this is also the case in the present system, where the reorientation from flat-lying to edge-on leads to a, on average, larger spatial distance between the substrate and the molecular core (i.e., it is π-system). Indeed, as a result of this larger distance, the net charge transfer for the edge-on configuration is even notably smaller than for the flat-lying geometry (see Figure 7c), despite a larger overall bond dipole. In turn, as a result of the smaller net charge transfer, the Fermi level lies below the peak of the LUMO-derived DOS feature for the standing layer, while it is above the peak for flat-lying NO_2-Pyt. This, together with an increased broadening of the peak in the upright-standing, case causes an additional work-function increase for that system.

IV. SUMMARY AND CONCLUSION

Employing complementary experimental and modeling techniques, we studied the geometry and electronic structure of pyrene derivatives with varying electron affinity adsorbed on Au(111) and Ag(111). The side-group functionalization increases the electron affinity in the order: PyT < Br-PyT < NO_2-PyT. The interaction of the molecules with the Au(111) surface is comparably weak and dominated by Pauli push-back, especially for PyT. Upon increasing the electron affinity to that of NO_2-PyT, a transition to weak chemisorptive interaction is observed, with (comparably minor) substrate-to-molecule electron transfer. Both the experimental and the computational results show that the adsorption-induced work function modification reproduces the trend of the isolated molecular electron affinity well, both qualitatively and quantitatively. In contrast, on Ag(111) we find strong chemical interaction between PyT, Br-PyT, NO_2-PyT, and the surface. Both valence band photoelectron spectroscopy data and simulations clearly demonstrate substantial electron transfer from the metal to the adsorbate in all three cases. XSW measurements and DFT modeling show that the carbonyl groups are bent toward the surface and have virtually identical bonding distances for all molecules, while the average bonding distances of the carbon skeletons are significantly different (Δ = 0.37 Å in the XSW experiments).

For the Br-PyT/Ag(111) and NO_2-PyT/Ag(111) interfaces, the experimental work function modification is extraordinarily large. The strongest increase is observed for NO_2-PyT, where the maximum absolute work function is determined to be 6.15 eV, which clearly exceeds the expectations based on the molecular properties. In fact, a work function of 6.15 eV for a Ag(111) substrate goes far beyond what has been obtained for other molecules with even higher electron affinities.[48,55] We suggest that the extremely large work function change for NO_2-PyT at 12 Å nominal coverage is due to an edge-on phase. For such a phase our simulations indeed show a massively increased work-function change compared to the face-on phase. Interestingly, this occurs in spite of the prevalence of Fermi-level pinning. This is explained as a consequence of the interfacial charge rearrangements in conjunction with the orientation-dependent electron affinity of the adsorbate layer. The fact that the edge-on phase is *not* observed in XSW experiments performed at much lower nominal coverage points to a coverage-dependent phase transition from face-on to edge-on.

Our results show that the interface energetics of metal/organic molecule contacts cannot be simply predicted from the electron affinities of the adsorbate molecules alone, although this parameter does significantly impact molecule−metal

DOI: 10.1021/acs.jpcc.7b08451
J. Phys. Chem. C 2017, 121, 24657−24668

interactions. As a consequence, high work function modifications become possible even with acceptors considered as only moderately interesting in view of their electron affinities. For NO_2-PyT on Ag(111) the reorientation in the monolayer (from face-on to edge-on) *de*creases the average electron transfer per molecule but *in*creases the work function. This is explained by a change of the electron affinity by reorientation and the increased length of the charge separation in the interfacial dipole. Thus, also for nonpolar acceptor molecules the orientation plays a crucial role, and for the employed acceptors, an edge-on orientation is beneficial for high substrate work functions. Consequently, adding anchoring groups to acceptors is a feasible tool for interface engineering also on practically more relevant electrodes than Ag(111).

■ ASSOCIATED CONTENT

Supporting Information

The Supporting Information is available free of charge on the ACS Publications website at DOI: 10.1021/acs.jpcc.7b08451.

Cyclic voltammetry data of PyT, Br-PyT, and NO_2-PyT; X-ray photoelectron spectroscopy data of PyT, Br-PyT, and NO_2-PyT on Au(111) and Ag(111), and ultraviolet photoelectron spectroscopy data of Br-PyT on Au(111) and Ag(111) (PDF)

■ AUTHOR INFORMATION

Corresponding Authors

*E-mail: o.hofmann@tugraz.at.
*E-mail: duhm@suda.edu.cn.

ORCID

O. T. Hofmann: 0000-0002-2120-3259
K. Müllen: 0000-0001-6630-8786
E. Zojer: 0000-0002-6502-1721
N. Koch: 0000-0002-6042-6447
S. Duhm: 0000-0002-5099-5929

Notes

The authors declare no competing financial interest.

■ ACKNOWLEDGMENTS

This work was financially supported by an NSFC Research Fund for International Young Scientists (No. 11550110176), the Soochow University-Western University Joint Center for Synchrotron Radiation Research, the Collaborative Innovation Center of Suzhou Nano Science and Technology (NANO−CIC), the 111 Project of the Chinese State Adminsitration of Foreign Experts Affairs, the Helmholtz Energy Alliance "Hybrid Photovoltaics", and the Collaborative Research Centre SFB951 of the German Research Foundation (DFG). We acknowledge the synchrotron radiation facilities -ESRF and BESSY II for provision of beamtime. The computational results were achieved in part using the Vienna Scientific Cluster (VSC). Funding by the Austrian Science Fund (FWF) (P27868−N36 and P24666−N20) is gratefully acknowledged; FS acknowledges funding from the DFG and IS support from the DFG project FoMEDOS (No. 624765). We also thank the Gutenberg Research Center for generous support.

■ REFERENCES

(1) Street, R. A. Electronic Structure and Properties of Organic Bulk-Heterojunction Interfaces. *Adv. Mater.* **2016**, *28*, 3814−3830.
(2) Ratcliff, E. L.; Zacher, B.; Armstrong, N. R. Selective Interlayers and Contacts in Organic Photovoltaic Cells. *J. Phys. Chem. Lett.* **2011**, *2*, 1337−1350.
(3) Nakano, K.; Tajima, K. Organic Planar Heterojunctions: From Models for Interfaces in Bulk Heterojunctions to High-Performance Solar Cells. *Adv. Mater.* **2017**, *29*, 1603269−33.
(4) Pelzer, K. M.; Darling, S. B. Charge generation in organic photovoltaics: a review of theory and computation. *Mol. Syst. Des. Eng.* **2016**, *1*, 10−24.
(5) Bröker, B.; Blum, R.-P.; Frisch, J.; Vollmer, A.; Hofmann, O. T.; Rieger, R.; Müllen, K.; Rabe, J. P.; Zojer, E.; Koch, N. Gold work function reduction by 2.2 eV with an air-stable molecular donor layer. *Appl. Phys. Lett.* **2008**, *93*, 243303−3.
(6) Hofmann, O. T.; Rangger, G. M.; Zojer, E. Reducing the Metal Work Function beyond Pauli Pushback: A Computational Investigation of Tetrathiafulvalene and Viologen on Coinage Metal Surfaces. *J. Phys. Chem. C* **2008**, *112*, 20357−20365.
(7) Meyer, J.; Hamwi, S.; Bulow, T.; Johannes, H.-H.; Riedl, T.; Kowalsky, W. Highly efficient simplified organic light emitting diodes. *Appl. Phys. Lett.* **2007**, *91*, 113506.
(8) Campbell, I. H.; Rubin, S.; Zawodzinski, T. A.; Kress, J. D.; Martin, R. L.; Smith, D. L.; Barashkov, N. N.; Ferraris, J. P. Controlling Schottky energy barriers in organic electronic devices using self-assembled monolayers. *Phys. Rev. B: Condens. Matter Mater. Phys.* **1996**, *54*, 14321−14324.
(9) Lee, H. J.; Jamison, A. C.; Lee, T. R. Surface Dipoles: A Growing Body of Evidence Supports Their Impact and Importance. *Acc. Chem. Res.* **2015**, *48*, 3007−3015.
(10) Heimel, G.; Romaner, L.; Zojer, E.; Brédas, J.-L. The Interface Energetics of Self-Assembled Monolayers on Metals. *Acc. Chem. Res.* **2008**, *41*, 721−729.
(11) Ishii, H.; Sugiyama, K.; Ito, E.; Seki, K. Energy Level Alignment and Interfacial Electronic Structures at Organic/Metal and Organic/Organic Interfaces. *Adv. Mater.* **1999**, *11*, 605−625.
(12) Koch, N.; Duhm, S.; Rabe, J. P.; Vollmer, A.; Johnson, R. L. Optimized Hole Injection with Strong Electron Acceptors at Organic-Metal Interfaces. *Phys. Rev. Lett.* **2005**, *95*, 237601−4.
(13) Otero, R.; Vázquez de Parga, A.; Gallego, J. Electronic, structural and chemical effects of charge-transfer at organic/inorganic interfaces. *Surf. Sci. Rep.* **2017**, *72*, 105−145.
(14) Tseng, T.-C.; et al. Charge-transfer-induced structural rearrangements at both sides of organic/metal interfaces. *Nat. Chem.* **2010**, *2*, 374−379.
(15) Romaner, L.; Heimel, G.; Brédas, J.-L.; Gerlach, A.; Schreiber, F.; Johnson, R. L.; Zegenhagen, J.; Duhm, S.; Koch, N.; Zojer, E. Impact of Bidirectional Charge Transfer and Molecular Distortions on the Electronic Structure of a Metal-Organic Interface. *Phys. Rev. Lett.* **2007**, *99*, 256801−4.
(16) Heimel, G.; et al. Charged and metallic molecular monolayers through surface-induced aromatic stabilization. *Nat. Chem.* **2013**, *5*, 187−194.
(17) Willenbockel, M.; Lüftner, D.; Stadtmüller, B.; Koller, G.; Kumpf, C.; Soubatch, S.; Puschnig, P.; Ramsey, M. G.; Tautz, F. S. The interplay between interface structure, energy level alignment and chemical bonding strength at organic-metal interfaces. *Phys. Chem. Chem. Phys.* **2015**, *17*, 1530−1548.
(18) He, Y.; Bussolotti, F.; Xin, Q.; Yang, J.; Kera, S.; Ueno, N.; Duhm, S. Transient Monolayer Structure of Rubrene on Graphite: Impact on Hole-Phonon Coupling. *J. Phys. Chem. C* **2016**, *120*, 14568−14574.
(19) Kowarik, S.; Gerlach, A.; Sellner, S.; Schreiber, F.; Cavalcanti, L.; Konovalov, O. Real-Time Observation of Structural and Orientational Transitions during Growth of Organic Thin Films. *Phys. Rev. Lett.* **2006**, *96*, 125504−4.
(20) Bröker, B.; Hofmann, O. T.; Rangger, G. M.; Frank, P.; Blum, R.-P.; Rieger, R.; Venema, L.; Vollmer, A.; Müllen, K.; Rabe, J. P.; Winkler, A.; Rudolf, P.; Zojer, E.; Koch, N. Density-Dependent Reorientation and Rehybridization of Chemisorbed Conjugated

Molecules for Controlling Interface Electronic Structure. *Phys. Rev. Lett.* **2010**, *104*, 246805−4.
(21) Marschall, M.; Reichert, J.; Diller, K.; Klyatskaya, S.; Ruben, M.; Nefedov, A.; Wöll, C.; Kantorovich, L. N.; Klappenberger, F.; Barth, J. V. Meta-Positioning of Carbonitrile Functional Groups Induces Interfacial Edge-On Phase of Oligophenyl Derivatives. *J. Phys. Chem. C* **2014**, *118*, 2622−2633.
(22) Maurer, R. J.; Ruiz, V. G.; Camarillo-Cisneros, J.; Liu, W.; Ferri, N.; Reuter, K.; Tkatchenko, A. Adsorption structures and energetics of molecules on metal surfaces: Bridging experiment and theory. *Prog. Surf. Sci.* **2016**, *91*, 72−100.
(23) Della Pia, A.; Riello, M.; Lawrence, J.; Stassen, D.; Jones, T. S.; Bonifazi, D.; De Vita, A.; Costantini, G. Two-Dimensional Ketone-Driven Metal-Organic Coordination on Cu(111). *Chem. - Eur. J.* **2016**, *22*, 8105−8112.
(24) Marder, S. R.; Kippelen, B.; Jen, A. K.-Y.; Peyghambarian, N. Design and synthesis of chromophores and polymers for electro-optic and photorefractive applications. *Nature* **1997**, *388*, 845−851.
(25) Serna, P.; Gates, B. C. Molecular Metal Catalysts on Supports: Organometallic Chemistry Meets Surface Science. *Acc. Chem. Res.* **2014**, *47*, 2612−2620.
(26) Li, Q.; Yang, B.; Lin, H.; Aghdassi, N.; Miao, K.; Zhang, J.; Zhang, H.; Li, Y.; Duhm, S.; Fan, J.; Chi, L. Surface-Controlled Mono/Diselective ortho C-H Bond Activation. *J. Am. Chem. Soc.* **2016**, *138*, 2809−2814.
(27) Naghavi, S. S.; Gruhn, T.; Alijani, V.; Fecher, G. H.; Felser, C.; Medjanik, K.; Kutnyakhov, D.; Nepijko, S. A.; Schönhense, G.; Rieger, R.; Baumgarten, M.; Müllen, K. Theoretical study of new acceptor and donor molecules based on polycyclic aromatic hydrocarbons. *J. Mol. Spectrosc.* **2011**, *265*, 95−101.
(28) Kawano, S.; Baumgarten, M.; Chercka, D.; Enkelmann, V.; Müllen, K. Electron donors and acceptors based on 2,7-functionalized pyrene-4,5,9,10-tetraone. *Chem. Commun.* **2013**, *49*, 5058−5060.
(29) Liang, Y.; Zhang, P.; Chen, J. Function-oriented design of conjugated carbonyl compound electrodes for high energy lithium batteries. *Chem. Sci.* **2013**, *4*, 1330−1337.
(30) Nokami, T.; Matsuo, T.; Inatomi, Y.; Hojo, N.; Tsukagoshi, T.; Yoshizawa, H.; Shimizu, A.; Kuramoto, H.; Komae, K.; Tsuyama, H.; Yoshida, J. Polymer-Bound Pyrene-4,5,9,10-tetraone for Fast-Charge and -Discharge Lithium-Ion Batteries with High Capacity. *J. Am. Chem. Soc.* **2012**, *134*, 19694−19700.
(31) Barathi, P.; Senthil Kumar, A. Electrochemical Conversion of Unreactive Pyrene to Highly Redox-Active 1,2-Quinone Derivatives on a Carbon Nanotube-Modified Gold Electrode Surface and Its Selective Hydrogen Peroxide Sensing. *Langmuir* **2013**, *29*, 10617−10623.
(32) Zegenhagen, J. Surface Structure Analysis with X-Ray Standing Waves. In *Springer Series in Surface Sciences*; Bracco, G., Holst, B., Eds.; Springer: Berlin Heidelberg, 2013; Vol. *51*; pp 249−275.
(33) Gerlach, A.; Bürker, C.; Hosokai, T.; Schreiber, F. X-Ray Standing Waves and Surfaces X-Ray Scattering Studies of Molecule-Metal Interfaces. In *The Molecule-Metal Interface*; Koch, N., Ueno, N., Wee, A. T. S., Eds.; Wiley-VCH, 2013; pp 153−172.
(34) Watson, M. D.; Fechtenkötter, A.; Müllen, K. Big Is Beautiful−Aromaticity Revisited from the Viewpoint of Macromolecular and Supramolecular Benzene Chemistry. *Chem. Rev.* **2001**, *101*, 1267−1300.
(35) Vollmer, A.; Jurchescu, O. D.; Arfaoui, I.; Salzmann, I.; Palstra, T. T. M.; Rudolf, P.; Niemax, J.; Pflaum, J.; Rabe, J. P.; Koch, N. The effect of oxygen exposure on pentacene electronic structure. *Eur. Phys. J. E: Soft Matter Biol. Phys.* **2005**, *17*, 339−343.
(36) Zegenhagen, J.; Detlefs, B.; Lee, T.-L.; Thiess, S.; Isern, H.; Petit, L.; André, L.; Roy, J.; Mi, Y. Y.; Joumard, I. X-ray standing waves and hard X-ray photoelectron spectroscopy at the insertion device beamline ID32. *J. Electron Spectrosc. Relat. Phenom.* **2010**, *178*−*179*, 258−267.
(37) Gerlach, A.; Schreiber, F.; Sellner, S.; Dosch, H.; Vartanyants, I. A.; Cowie, B. C. C.; Lee, T.-L.; Zegenhagen, J. Adsorption-induced distortion of $F_{16}CuPc$ on Cu(111) and Ag(111): An x-ray standing wave study. *Phys. Rev. B: Condens. Matter Mater. Phys.* **2005**, *71*, 205425−7.
(38) Gerlach, A.; Sellner, S.; Schreiber, F.; Koch, N.; Zegenhagen, J. Substrate-dependent bonding distances of PTCDA: A comparative x-ray standing-wave study on Cu(111) and Ag(111). *Phys. Rev. B: Condens. Matter Mater. Phys.* **2007**, *75*, 045401−7.
(39) Blum, V.; Gehrke, R.; Hanke, F.; Havu, P.; Havu, V.; Ren, X.; Reuter, K.; Scheffler, M. Ab initio molecular simulations with numeric atom-centered orbitals. *Comput. Phys. Commun.* **2009**, *180*, 2175−2196.
(40) Perdew, J. P.; Burke, K.; Ernzerhof, M. Generalized Gradient Approximation Made Simple. *Phys. Rev. Lett.* **1996**, *77*, 3865−3868.
(41) Tkatchenko, A.; Scheffler, M. Accurate Molecular Van Der Waals Interactions from Ground-State Electron Density and Free-Atom Reference Data. *Phys. Rev. Lett.* **2009**, *102*, 073005−4.
(42) Ruiz, V. G.; Liu, W.; Zojer, E.; Scheffler, M.; Tkatchenko, A. Density-Functional Theory with Screened van der Waals Interactions for the Modeling of Hybrid Inorganic-Organic Systems. *Phys. Rev. Lett.* **2012**, *108*, 146103−5.
(43) Mori-Sanchez, P.; Cohen, A. J.; Yang, W. Many-electron self-interaction error in approximate density functionals. *J. Chem. Phys.* **2006**, *125*, 201102−4.
(44) Perdew, J. P.; Zunger, A. Self-interaction correction to density-functional approximations for many-electron systems. *Phys. Rev. B: Condens. Matter Mater. Phys.* **1981**, *23*, 5048−5079.
(45) Neaton, J. B.; Hybertsen, M. S.; Louie, S. G. Renormalization of Molecular Electronic Levels at Metal-Molecule Interfaces. *Phys. Rev. Lett.* **2006**, *97*, 216405−4.
(46) Garcia-Lastra, J. M.; Rostgaard, C.; Rubio, A.; Thygesen, K. S. Polarization-induced renormalization of molecular levels at metallic and semiconducting surfaces. *Phys. Rev. B: Condens. Matter Mater. Phys.* **2009**, *80*, 245427−7.
(47) Thygesen, K. S.; Rubio, A. Renormalization of Molecular Quasiparticle Levels at Metal-Molecule Interfaces: Trends across Binding Regimes. *Phys. Rev. Lett.* **2009**, *102*, 046802−4.
(48) Rangger, G. M.; Hofmann, O. T.; Romaner, L.; Heimel, G.; Bröker, B.; Blum, R.-P.; Johnson, R. L.; Koch, N.; Zojer, E. F4TCNQ on Cu, Ag, and Au as prototypical example for a strong organic acceptor on coinage metals. *Phys. Rev. B: Condens. Matter Mater. Phys.* **2009**, *79*, 165306−12.
(49) Hofmann, O. T.; Atalla, V.; Moll, N.; Rinke, P.; Scheffler, M. Interface dipoles of organic molecules on Ag(111) in hybrid density-functional theory. *New J. Phys.* **2013**, *15*, 123028−25.
(50) Neugebauer, J.; Scheffler, M. Adsorbate-substrate and adsorbate-adsorbate interactions of Na and K adlayers on Al(111). *Phys. Rev. B: Condens. Matter Mater. Phys.* **1992**, *46*, 16067−16080.
(51) Kokalj, A. Computer graphics and graphical user interfaces as tools in simulations of matter at the atomic scale. *Comput. Mater. Sci.* **2003**, *28*, 155−168.
(52) Kahn, A.; Koch, N.; Gao, W. Y. Electronic structure and electrical properties of interfaces between metals and π-conjugated molecular films. *J. Polym. Sci., Part B: Polym. Phys.* **2003**, *41*, 2529−2548.
(53) Bagus, P. S.; Staemmler, V.; Wöll, C. Exchange-like Effects for Closed-Shell Adsorbates: Interface Dipole and Work Function. *Phys. Rev. Lett.* **2002**, *89*, 096104−4.
(54) Toyoda, K.; Hamada, I.; Lee, K.; Yanagisawa, S.; Morikawa, Y. Density functional theoretical study of pentacene/noble metal interfaces with van der Waals corrections: Vacuum level shifts and electronic structures. *J. Chem. Phys.* **2010**, *132*, 134703−10.
(55) Duhm, S.; Glowatzki, H.; Rabe, J. P.; Koch, N.; Johnson, R. L. Spontaneous charge transfer at organic-organic homointerfaces to establish thermodynamic equilibrium. *Appl. Phys. Lett.* **2007**, *90*, 122113.
(56) Duhm, S.; Bürker, C.; Hosokai, T.; Gerlach, A. Vertical Bonding Distances Impact Organic-Metal Interface Energetics. In *Springer Series in Materials Science*; Ishii, H., Kudo, K., Nakayama, T., Ueno, N., Eds.; Springer: Japan, 2015; Vol. *209*; pp 89−107.

DOI: 10.1021/acs.jpcc.7b08451
J. Phys. Chem. C 2017, 121, 24657−24668

(57) Koch, N. Energy levels at interfaces between metals and conjugated organic molecules. *J. Phys.: Condens. Matter* **2008**, *20*, 184008−12.
(58) Hill, I. G.; Mäkinen, A. J.; Kafafi, Z. H. Initial stages of metal/organic semiconductor interface formation. *J. Appl. Phys.* **2000**, *88*, 889−895.
(59) Glowatzki, H.; Bröker, B.; Blum, R.-P.; Hofmann, O. T.; Vollmer, A.; Rieger, R.; Müllen, K.; Zojer, E.; Rabe, J. P.; Koch, N. Soft" Metallic Contact to Isolated C60 Molecules. *Nano Lett.* **2008**, *8*, 3825−3829.
(60) Duhm, S.; Gerlach, A.; Salzmann, I.; Bröker, B.; Johnson, R. L.; Schreiber, F.; Koch, N. PTCDA on Au(111), Ag(111) and Cu(111): Correlation of interface charge transfer to bonding distance. *Org. Electron.* **2008**, *9*, 111−118.
(61) Franco-Cañellas, A.; Wang, Q.; Broch, K.; Duncan, D. A.; Thakur, P. K.; Liu, L.; Kera, S.; Gerlach, A.; Duhm, S.; Schreiber, F. Metal-organic interface functionalization via acceptor end groups: PTCDI on coinage metals. *Phys. Rev. Materials* **2017**, *1*, 013001−6.
(62) Yonezawa, K.; Suda, Y.; Yanagisawa, S.; Hosokai, T.; Kato, K.; Yamaguchi, T.; Yoshida, H.; Ueno, N.; Kera, S. Charge transfer states appear in the pi-conjugated pure hydrocarbon molecule on Cu(111). *Appl. Phys. Express* **2016**, *9*, 045201−4.
(63) Hosokai, T.; Yonezawa, K.; Yang, J.; Koswattage, K.; Kera, S. Significant reduction in the hole-injection barrier by the charge-transfer state formation: Diindenoperylene contacted with silver and copper electrodes. *Org. Electron.* **2017**, *49*, 39−44.
(64) Hofmann, O. T.; Egger, D. A.; Zojer, E. Work-Function Modification beyond Pinning: When Do Molecular Dipoles Count? *Nano Lett.* **2010**, *10*, 4369−4374.
(65) Goiri, E.; Borghetti, P.; El-Sayed, A.; Ortega, J. E.; de Oteyza, D. G. Multi-Component Organic Layers on Metal Substrates. *Adv. Mater.* **2016**, *28*, 1340−1368.
(66) Yamane, H.; Gerlach, A.; Duhm, S.; Tanaka, Y.; Hosokai, T.; Mi, Y. Y.; Zegenhagen, J.; Koch, N.; Seki, K.; Schreiber, F. Site-Specific Geometric and Electronic Relaxations at Organic-Metal Interfaces. *Phys. Rev. Lett.* **2010**, *105*, 046103−4.
(67) Woodruff, D. P. Surface structure determination using x-ray standing waves. *Rep. Prog. Phys.* **2005**, *68*, 743−798.
(68) Zegenhagen, J. Surface structure determination with X-ray standing waves. *Surf. Sci. Rep.* **1993**, *18*, 202−271.
(69) Stadtmüller, B.; Schröder, S.; Kumpf, C. Heteromolecular metal-organic interfaces: Electronic and structural fingerprints of chemical bonding. *J. Electron Spectrosc. Relat. Phenom.* **2015**, *204*, 80−91.
(70) Bürker, C.; Ferri, N.; Tkatchenko, A.; Gerlach, A.; Niederhausen, J.; Hosokai, T.; Duhm, S.; Zegenhagen, J.; Koch, N.; Schreiber, F. Exploring the bonding of large hydrocarbons on noble metals: Diindoperylene on Cu(111), Ag(111), and Au(111). *Phys. Rev. B: Condens. Matter Mater. Phys.* **2013**, *87*, 165443−5.
(71) Yang, A.; et al. Nitrogen substitution impacts organic-metal interface energetics. *Phys. Rev. B: Condens. Matter Mater. Phys.* **2016**, *94*, 155426−9.
(72) Duhm, S.; Bürker, C.; Niederhausen, J.; Salzmann, I.; Hosokai, T.; Duvernay, J.; Kera, S.; Schreiber, F.; Koch, N.; Ueno, N.; Gerlach, A. Pentacene on Ag(111): Correlation of Bonding Distance with Intermolecular Interaction and Order. *ACS Appl. Mater. Interfaces* **2013**, *5*, 9377−9381.
(73) Hauschild, A.; Karki, K.; Cowie, B. C. C.; Rohlfing, M.; Tautz, F. S.; Sokolowski, M. Molecular Distortions and Chemical Bonding of a Large π-Conjugated Molecule on a Metal Surface. *Phys. Rev. Lett.* **2005**, *94*, 036106−4.
(74) Hauschild, A.; Temirov, R.; Soubatch, S.; Bauer, O.; Schöll, A.; Cowie, B. C. C.; Lee, T.-L.; Tautz, F. S.; Sokolowski, M. Normal-incidence x-ray standing-wave determination of the adsorption geometry of PTCDA on Ag(111): Comparison of the ordered room-temperature and disordered low-temperature phases. *Phys. Rev. B: Condens. Matter Mater. Phys.* **2010**, *81*, 125432−12.
(75) Scherbela, M.; Hörmann, L.; Obersteiner, V.; Hofmann, O. T. Leaving the Valley: Charting the Energy Landscape of Metal/Organic Interfaces via Machine Learning. *ArXiv e-prints* 2017, arXiv:1709.05417.
(76) Packwood, D. M.; Han, P.; Hitosugi, T. Chemical and entropic control on the molecular self-assembly process. *Nat. Commun.* **2017**, *8*, 14463−8.
(77) Obersteiner, V.; Scherbela, M.; Hörmann, L.; Wegner, D.; Hofmann, O. T. Structure Prediction for Surface-Induced Phases of Organic Monolayers: Overcoming the Combinatorial Bottleneck. *Nano Lett.* **2017**, *17*, 4453−4460.
(78) Hollerer, M.; Lüftner, D.; Hurdax, P.; Ules, T.; Soubatch, S.; Tautz, F. S.; Koller, G.; Puschnig, P.; Sterrer, M.; Ramsey, M. G. Charge Transfer and Orbital Level Alignment at Inorganic/Organic Interfaces: The Role of Dielectric Interlayers. *ACS Nano* **2017**, *11*, 6252−6260.
(79) Heimel, G.; Salzmann, I.; Duhm, S.; Koch, N. Design of Organic Semiconductors from Molecular Electrostatics. *Chem. Mater.* **2011**, *23*, 359−377.
(80) Duhm, S.; Heimel, G.; Salzmann, I.; Glowatzki, H.; Johnson, R. L.; Vollmer, A.; Rabe, J. P.; Koch, N. Orientation-dependent ionization energies and interface dipoles in ordered molecular assemblies. *Nat. Mater.* **2008**, *7*, 326−332.
(81) Yang, J.-P.; Bussolotti, F.; Kera, S.; Ueno, N. Origin and role of gap states in organic semiconductor studied by UPS: as the nature of organic molecular crystals. *J. Phys. D: Appl. Phys.* **2017**, *50*, 423002.
(82) Oehzelt, M.; Koch, N.; Heimel, G. Organic semiconductor density of states controls the energy level alignment at electrode interfaces. *Nat. Commun.* **2014**, *5*, 4174−8.

DOI: 10.1021/acs.jpcc.7b08451
J. Phys. Chem. C 2017, 121, 24657−24668